Effects of Retinoic Acid Dynamics on NTERA-2 Neuronal Differentiation

The University Of Sheffield.

Student: Chenpei Liu, Supervisor: Heather McCourty, Primary Supervisor: Anton Nikolaev
School of Biosciences, The University of Sheffield

SURE Sheffield Undergraduate Research Experience

INTRODUCTION

Background:
Ntera-2 (NT2) cells, as seen in Fig.1, are derived from the human testicular embryonal carcinoma. The line is pluripotent and exhibit properties of embryonic stem cells, such as a high nucleo-cytoplasmic ratio and expression of surface antigens SSEA-1 and TRA-1-60 (Andrews, 1984). These cells can undergo neuronal differentiation when exposed to retinoic acid (RA), as evidenced by neurite formation and the expression of neuronal markers (Lee and Andrews, 1960), as seen in Fig.2.

Challenge of current developmental neurobiology research:
The differentiation process is regulated by complex signalling networks, notably the ERK/MAPK and TGF-β pathways, which are critical in determining cell fate (Okita and Yamanaka, 2006; Levine, Lin, and Elowitz, 2013). Although the standard protocol for NT2 cell differentiation is six weeks, there is potential for optimization, particularly in the frequency of RA application. Consistency and scalability in differentiation protocols are essential for clinical translation and reducing heterogeneity of cell cultures (Di Nardo and Parker, 2011; Cao et al., 2021).

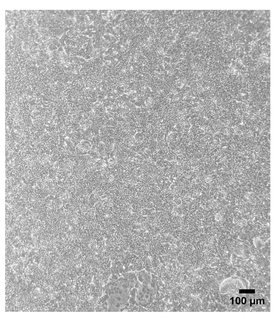

Fig.1: Undifferentiated Ntera-2 cells show a high nuclei to cytoplasm ratio (Andrews, 1984)

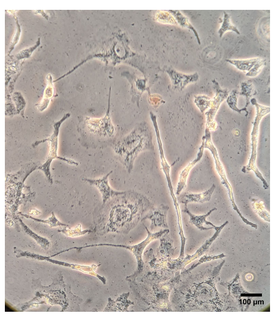

Fig.2: Differentiated Ntera-2 cells show their unique neuronal feature of elongated shapes for future axon development.

AIMS

- To automate NT2 differentiation using RA and a robotic platform (Katunin *et al.*, 2021) and optimise the automated protocol by varying RA conditions and collect high-throughput data.
- To assess differentiation using immunocytochemistry with TRA-1-60, a pluripotent cell surface marker, and A2B5, an early marker in neuronal cell fate, though not neuron-specific (Draper et al., 2002).

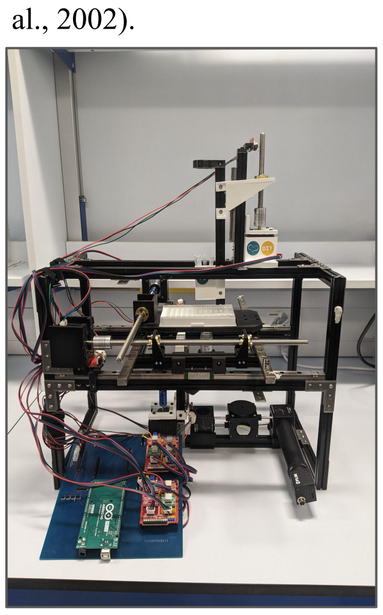

Fig.3: Assembled robot is designed in Fusion 360. Three stepper motors for X, Y and Z axis controls the movement of the plate. Up to eight capillaries can be used with the manifold to allow the Z-axis movement. Solutions of media and RA can be applied and removed with peristaltic pumps (Katunin *et al.*, 2021).

METHOD

1. The robotic platform was built as described by Katunin *et al.*, (2021), as seen in Fig.3.
2. A calibration protocol ran for 44 hours to test for a reliable pumping system for long-term experiments. Red and blue dyes were utilised to test pumping efficiency then the images captured beneath the plate. Images were processed in Lightroom, ImageJ and data analysis in R Studio. Fig.4 illustrates the calibration analysis workflow.
3. A serial dilution of AlexaFluor488 secondary antibody was established to identify optimal concentration for signal/noise ratio of fluorescent microscopic imaging. Results can be seen in Fig.6.
4. The protocol of cycling RA (10^{-5} M) and media was written in Python and automated by the robot in a CO_2 incubator for 7 days. Hoechst 3342, A2B5, and TRA-1-60 were used for immunolabeling to quantify cell changes.
5. Plates were imaged using InCell Analyzer 2200 and nuclei were segmented in Cellpose (Stringer *et al*, 2021). Data was visualised in R Studio. The analysis workflow can be seen in Fig.8 and results in Fig.9.

RESULTS

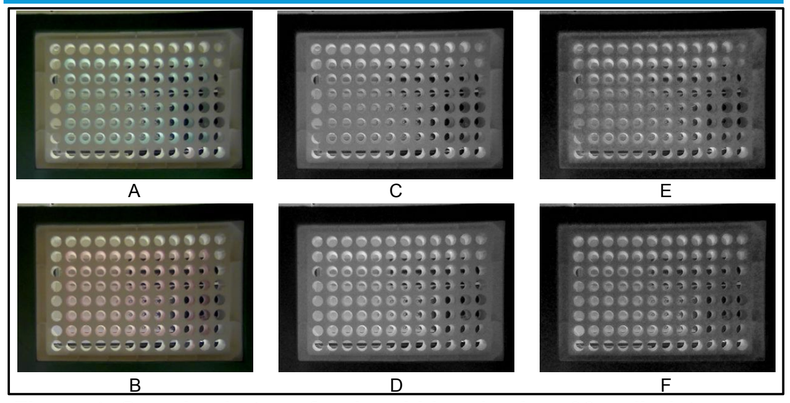

Figure 4: Sample photos of red and blue dye in a 96-well plate were split into red and blue channels to quantify the results of the calibration experiment.
- In the RGB channel (Fig.4 A, B), the images show plate with red or blue dye. This suggests the robot has been successful in addition and removal of the solution in each cell wells.
- In the colour split channels (Fig.4 C, D, E, F), the images show the grey intensity of the split channels to quantify the efficiency of the dye application. Lack of purple dye suggests successful dye addition and removal.

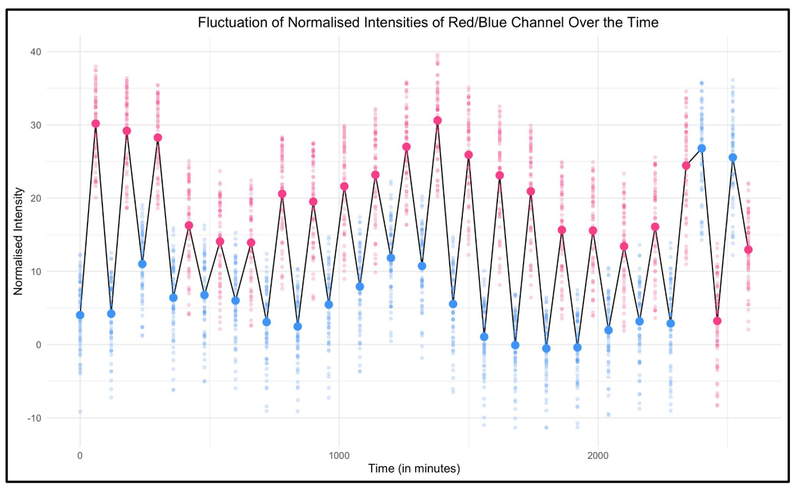

Figure 5: Visualisation of quantified calibration test results shows a relative stable fluctuation of intensities of channels, suggesting a successful cycling of the dyes. Data is presented as average normalised intensities with semi-transparent individual intensities.
- Red channel intensity is deducted by the blue channel intensity for each photo to obtain normalised intensities for clearer fluctuations.

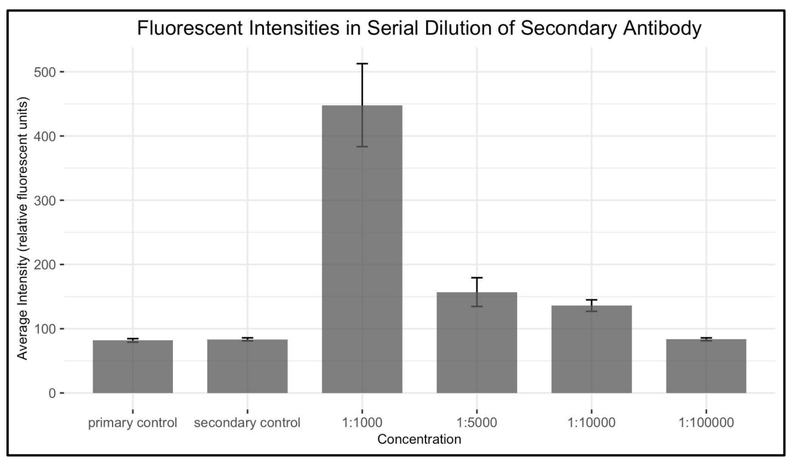

Fig. 6: Fluorescent intensities in a serial dilution of secondary antibody (AlexaFluor488) on undifferentiated NT2 cells (TRA-1-60 as primary antibody) with two control groups shows 1:1000 provides the best signal/noise ratio. Data is presented as average relative fluorescent intensities of each image analysed.
- Error bars are based on the standard error of the means within each group, though 1:1000 shows the highest variation.
- Primary and secondary control represents the group labelled with only primary and only secondary antibody, respectively.

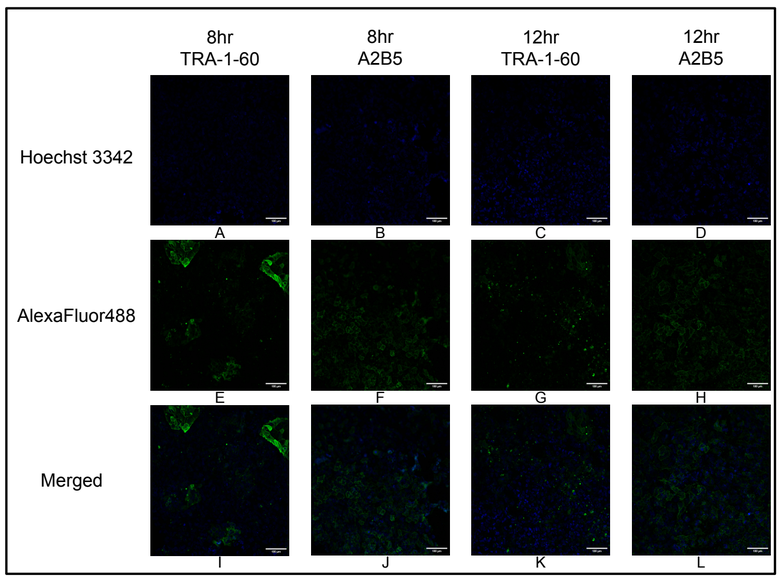

Fig. 7: Sample fluorescent images of Ntera-2 cells under 8-hour and 12-hour RA cycling condition was immunolabelled by differentiation marker, A2B5 and pluripotent marker, TRA-1-60
- Hoechst 3342 stains the nucleus (Fig.7A, B, C and D) which is used to segment and generate a mask (Fig.8C).
- A clear difference can be observed in expression of TRA-1-60 (Fig.7E compared to 7G) and A2B5 (Fig.7F compared to 7H) in the 8 hour and 12-hour conditions.

RESULTS

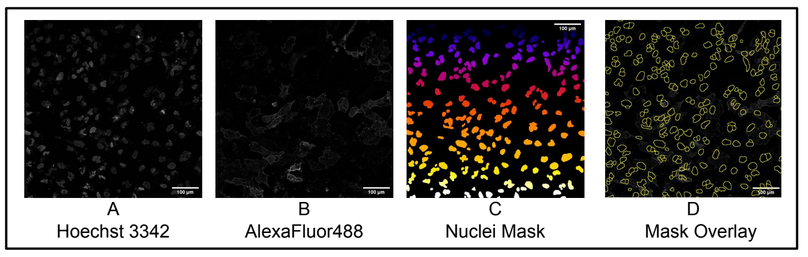

Fig. 8: Sample workflow of intensity data processing was performed using cellpose and Python. Segmentation of the cells was acquired in cellpose and then analysed in Python.
- In cellpose, pre-trained neural network counts the number of cells and identifies the pixel coordinates of the cells in each image captured.
- The pixel coordinates from the mask are used to measure average intensity over the masked locations in the AlexaFluor488 channel. Then an average fluorescence intensities over the nucleus are obtained, which examines whether cells are positive or negative for the selected antigen.
- The area of each nucleus and its eccentricity can also be measured and used to further analyse the differentiation.

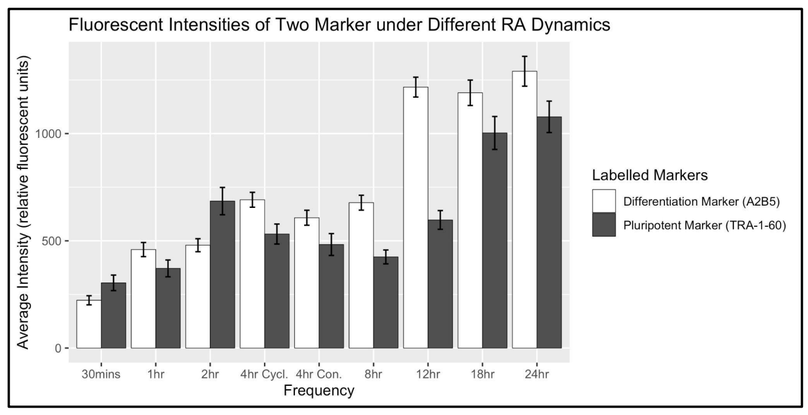

Fig. 9: Fluorescent intensities of cells labelled with TRA-1-60 and A2B5 after 7-days differentiation with RA at various frequencies shows an overall increasing trend in expression of both markers as cycling time increases. Data is presented as average relative fluorescent intensities of each segmented cell.
- Error bars illustrate the standard error of the means within each group.
- Application of RA was conducted at different frequencies, every 30 minutes, 1, 2, 4, 8, 12, 18 and 24 hours. For the 4-hour conditions, RA was either applied constantly (4hr Con.) or cycled (4hr Cycl.).
- A One-way ANOVA was used to test for significant difference between each frequency, within its selected antigen group. The results for both A2B5 ($p=7.77>0.05$) and TRA-1-60 ($p=10.31>0.05$) markers indicate significant differences between different RA cycling conditions.
- Tukey Post-hoc test was used to find specific differences between nine frequency groups. The 18-hour and 24-hour conditions for TRA-1-60 expression were significantly different to all other conditions, but not between each other. For A2B5 expression, the 12, 18 and 24-hour were significantly different to all other conditions, but not between each other. This suggests that cycling RA every 12, 18 and 24 hours have significantly higher expression of A2B5.

.

CONCLUSION

- Quantified results of solution cycling has evidenced the reliability of the assembled robot to automate long-term experiment protocols.
- Data analysis of current fluorescent intensity results reveals that cycling retinoic acid may affect A2B5 expression during Ntera-2 cell differentiation.

Future experiments will focus on
- Conduct experiments with varying doses of RA and more specific RA cycling frequencies.
- Refine the algorithms to increase the accuracy of fluorescent intensities to ensure that the data captured is representative of the actual conditions.
- Automate the recognition of neuronal morphology to expedite the analysis process and reduce the working load of manual cell segmentation.

REFERENCE

- Andrews, P. W. (1984) 'Retinoic acid induces neuronal differentiation of a cloned human embryonal carcinoma cell line in vitro', Developmental biology, 103(2), pp. 285–293. doi: 10.1016/0012-1606(84)90316-6.
- Cao, J. et al. (2021) 'Developing standards to support the clinical translation of stem cells', Stem Cells Translational Medicine, 10(Suppl 2), pp. S85–S95. doi:10.1002/sct3.13035.Lee, V.M. and Andrews, P.W., 1986. Differentiation of NTERA-2 clonal human embryonal carcinoma cells into neurons involves the induction of all three neurofilament proteins. J Neurosci, 6(2), pp.514-521. Available at: DOI: 10.1523/jneurosci.06-02-00514.1986
- Draper, J. S. et al. (2002) 'Surface antigens of human embryonic stem cells: changes upon differentiation in culture', Journal of anatomy, 200(3), pp. 249–258. doi: 10.1046/j.1469-7580.2002.00030.x.
- Katunin, P. et al. (2021) 'An Open-Source Framework for Automated High-Throughput Cell Biology Experiments', Frontiers in Cell and Developmental Biology, 9. Available at: https://www.frontiersin.org/article/10.3389/fcell.2021.697584.
- Lee, V.M. and Andrews, P.W., 1986. Differentiation of NTERA-2 clonal human embryonal carcinoma cells into neurons involves the induction of all three neurofilament proteins. J Neurosci, 6(2), pp.514-521. Available at: DOI: 10.1523/jneurosci.06-02-00514.1986
- Levine, J.H., Lin, Y. and Elowitz, M.B. (2013) 'Functional roles of pulsing in genetic circuits', Science (New York, N.Y.), 342(6163), pp. 1193–1200. Available at: https://doi.org/10.1126/science.1239999.
- Nardo, P.D. and Parker, G.C. (2011) Stem Cell Standardization, https://home.liebertpub.com/scd. Mary Ann Liebert, Inc. 140 Huguenot Street, 3rd Floor New Rochelle, NY 10801 USA. doi:10.1089/scd.2011.1500.
- Okita, K. and Yamanaka, S. (2006) 'Intracellular Signaling Pathways Regulating Pluripotency of Embryonic Stem Cells', Current Stem Cell Research & Therapy, 1(1), pp. 103–111.
- Raina, D. et al. (2022) 'Intermittent ERK oscillations downstream of FGF in mouse embryonic stem cells', Development, 149(4), p. dev199710. Available at: https://doi.org/10.1242/dev.199710.
- Stringer, C. et al. (2021) 'Cellpose: a generalist algorithm for cellular segmentation', Nature methods, 18(1), pp. 100–106. doi: 10.1038/s41592-020-01018-x.
- Thomson, J.A. *et al.* (1998) 'Embryonic stem cell lines derived from human blastocysts', *Science (New York, N.Y.)*, 282(5391), pp. 1145–1147. Available at: https://doi.org/10.1126/science.282.5391.1145.